ACS OMEGA

Open Access

http://pubs.acs.org/journal/acsodf

Article

Silk Fibroin Improves the Biological Properties of Egg White-Based Bioink for the Bioprinting of Tissue Engineering Materials

Hai-Yan Wang,[§] Shu-Xiang Zhao,[§] Ji-Xin Li, and Yu-Qing Zhang*

Cite This: *ACS Omega* 2023, 8, 46685−46696

Read Online

ACCESS | Metrics & More | Article Recommendations

ABSTRACT: Egg white (EW) is a common nutritious food with excellent heat gelation and biocompatibility, but its application in biomaterials is considerably limited. Silk fibroin (SF) is a protein-based fiber with both excellent mechanical properties and biocompatibility, and its application in biomaterials has attracted much attention. Here, the EW/SF composite scaffold was first synthesized with GMA-modified EW/SF composite bioink (G-EW/SF). When homogenized EW and SF were individually grafted with glycidyl methacrylate (GMA), the grafted EW (G-EW) and SF (G-SF) were mixed in different proportions and then added to I2959. The resulting G-EW/SF composite bioink could be bioprinted into various EW/SF composite scaffolds. Among them, the compressive modulus of EW/SF (50%) composite scaffolds incorporating 50% G-SF was significantly improved. It had a three-dimensional (3D) polypore structure with an average pore size of 61 μm and was mainly composed of β-sheet structures. Compared with the EW scaffold alone, the thermal decomposition temperature of the EW/SF scaffold was 10 °C higher, and the residual rate after 9 days of enzymatic hydrolysis had increased by about 18%. The scaffold prolonged the sustained release of insulin and promoted the adhesion, growth, and proliferation of the L-929 cells. Therefore, the EW/SF composite scaffolds with good cell proliferation ability and certain mechanical properties can be used in different applications including cells, drugs, and tissues. These results provide new prospects for the application of the EW protein to medical tissue engineering materials.

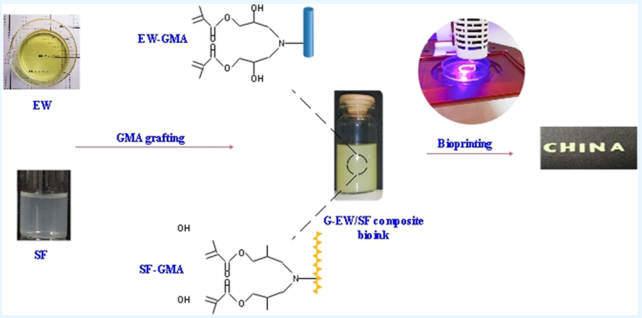

1. INTRODUCTION

Bioink mainly used for three-dimensional (3D) printing is often mixed with living cells; therefore, it should not initially be toxic to cells. A bioprinted scaffold, after printing and solidification, has certain mechanical properties, which can be slowly degraded in the body, and the embedded cells can grow freely. The bioink should promote cell adhesion, growth, and proliferation.[1] Bioinks play an important role in the field of bioprinting, and despite the variety of synthetic polymers, their poor biocompatibility hinders the further development of bioinks. Therefore, it is crucial to develop novel and excellent bioinks.

Compared with other biological materials, egg white (EW) is easy to obtain, widely available, and affordable. EW is a nutritionally balanced food and contains all of the essential amino acids, and almost 100% of it is absorbed by the human body.[2] Because of its emulsification, heat setting, gelation, and bonding properties,[3,4] EW is often used as an additive in nutritious food.[5] EW influences primitive biology and embryonic development.[6] Only about 15% of EW is solid matter, of which 80% is proteins, specifically ovalbumin, ovotransferrin, and ovomucoid. The molecular weight of these proteins varies greatly, ranging from 1.27 to 800 kDa. The hydrolysates of various proteins in EW have the potential to be widely used in the pharmaceutical, nutrition, and food industries. EW has many functions such as antioxidation,[7] immune regulation,[8] antibacterial activity,[9] wound healing,[10] antitumor activity,[11] and lowering blood sugar.[12]

Under the action of ultrasonication, EW can form nanoparticles for embedding drugs to treat cancer.[13] Because the biological materials made of EW protein are easy to degrade and show weak mechanical properties and poor water resistance, EW is often mixed with polymer materials such as alginate, cellulose, poly(vinyl alcohol), and so on to prepare scaffold materials.[14−16] The EW and sodium alginate nanoparticles loaded with paclitaxel can be easily prepared by an electronic spray method. The nanoparticles exhibit excellent particle size dispersion, uniform morphology, effective drug release performance, favorable biocompatibility, and can effectively inhibit CT26 colorectal cancer cells *in vitro*[17] In

Received: August 7, 2023
Revised: November 5, 2023
Accepted: November 16, 2023
Published: November 27, 2023

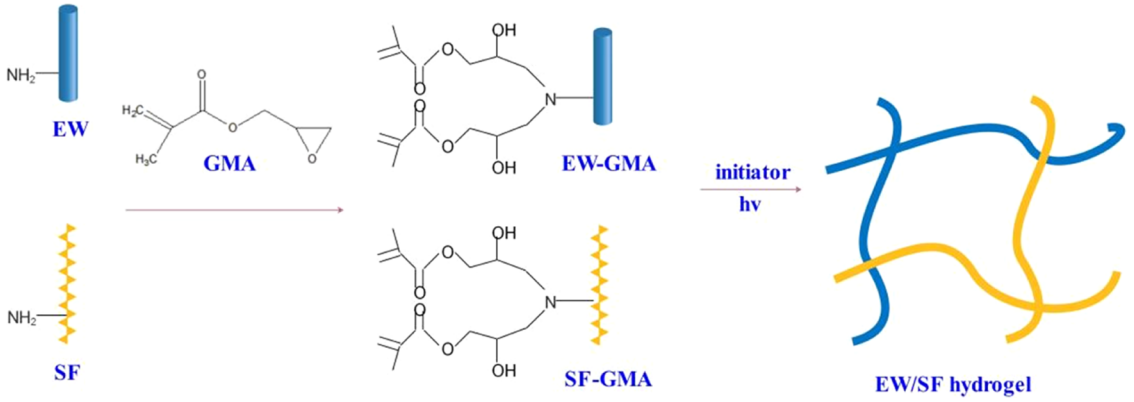

Figure 1. Schematic diagram of the preparation of the EW/SF bioink.

addition, the mechanical properties of EW materials also can be improved through cross-linking. With the addition of cross-linking agents such as methyl vinyl ether-maleic acid, carbodiimide, and glutaraldehyde, EW can form 3D scaffold materials with improved mechanical properties, which can promote cell adhesion and regeneration.[18−20] Duan et al.[21] used sodium hydroxide to induce the gelation of EW and subsequently introduced calcium ions to cross-link with EW protein chains to prepare a dual cross-linked hydrogel. This hydrogel exhibited biocompatibility and cell-surface adhesion *in vitro* and showed potential for use in bone tissue engineering. In addition, EW, gelatin, corn starch, and sucrose can be mixed to print a complex 3D scaffold by melt extrusion, which is expected to be useful in medical tissue engineering materials.[22] With the addition of gelatin methacryloyl, EW and eggshells can form biomimetic hybrid hydrogels with simple photopolymerization by UV irradiation. The hybrid hydrogels have effects on macrophages and can regulate the osteogenic differentiation of human dental pulp stem cells, which show potential for enhanced bone regeneration.[23]

Silk fibroin (SF) is a natural protein produced by silkworm *Bombyx mori*. SF has been widely explored as a bioactive and biomedical material due to its biocompatibility and superior mechanical properties.[24] Its excellent biological properties, such as chemical modification and conformational transformation induction, make it a biological ink with good bioprinting ability.[25] It has been reported that SF chemically modified with methacrylic anhydride (MA) or glycidyl methacrylate (GMA) can be cured into a new type of hydrogel under ultraviolet light in the presence of a photoinitiator, and the amount of SF can adjust its mechanical and rheological properties added.[26] In addition, these SF scaffolds can satisfy the adhesion, migration, and proliferation of L-929 cells, implying that the MA- or GMA-modified SF bioinks may be adapted to a variety of applications, including cells, drugs, tissues, etc.[27]

As mentioned above, the EW exhibits excellent biological properties. However, there is a paucity of literature regarding its utilization in the preparation of bioink. The EW proteins contain lysine residues and possess the potential to undergo modification by MA or GMA, enabling them to undergo photocuring and form gels (Figure 1). In order to improve the mechanical properties of EW materials, SF is introduced into EW to prepare a G-EW/SF composite ink with improved 3D mechanical properties (Figure 1). The preparation process, mechanical properties, resistance to enzymatic hydrolysis, and cytocompatibility of this G-EW/SF composite ink are systematically investigated in this study.

2. EXPERIMENTAL MATERIALS AND METHODS

2.1. Materials and Instruments. Silkworm cocoons (produced in the spring of 2018) were purchased from Jiangsu Nantong New Silk Road Silk, and the silkworm species was "Suhao × Zhongye". The Lan Fe brand of chicken eggs is produced in Shanghai by Dahe Egg Products Co., Ltd. (Shanghai, China). The mouse fibroblast L-929 was purchased from Procell Life Science & Technology Co., Ltd.

2.2. Bioink Synthesis Method. *2.2.1. Silk Degumming.* The degumming of the silkworm cocoon shells and silk fibers was performed according to our reported method.[28] The cocoon shells were boiled in an aqueous solution of 0.025% (w/v) calcium hydroxide for 20 min twice (bath ratio 1:60). The resulting SF fibers were washed repeatedly with deionized water, dried at 90 °C for 4 h, sealed, and protected from light for later use.

2.2.2. EW Purification. After the eggs were broken, the egg white was collected using an EW separator and poured into the tank of an electric grinder for intermittent high-speed shearing (500−5000 rpm, 1−5 min). Then, the sheared EW homogenate was centrifuged (10,000 rpm, 30 min), and the supernatant was recovered as homogenized EW, which was stored at 4 °C before use.

2.2.3. Modification Reaction. The dried SF obtained by degumming with slaked limewater was dissolved and grafted with GMA according to the method reported by Kim et al.[26] The SF salt solution was placed on a magnetic stirrer, and GMA was slowly added dropwise to the SF salt solution at a rate of about 0.5 mL/min. The grafting conditions were as follows: the speed was 300 rpm, the temperature was 60 °C, and the time was 3 h. Then, the grafted solution was transferred to a dialysis bag (MW: 14000) and dialyzed for 3 days, during which deionized water was changed every 6 h. Finally, GMA-grafted SF (G-SF) was frozen at −80 °C, then dried into a porous foamlike structure using a freeze-dryer, and stored in the dark.

The concentration of the homogenate (about 13%) was determined by the gravimetric method, then it was diluted to 10% (w/v) and transferred to a magnetic stirrer, and 1.0, 2.5, 5.0, and 7.5 mL of GMA was slowly added dropwise at a rate of about 0.5 mL/min into 100 mL of the EW solution (10%, w/v). The grafting conditions were a rotation speed of 300 rpm, a temperature of 25 °C, and a duration of 3 h. The

https://doi.org/10.1021/acsomega.3c05810
ACS Omega 2023, 8, 46685−46696

remaining steps were the same as those for making G-SF to obtain the grafted EW (G-EW). Among them, the four kinds of grafted EW resulting from different volumes of G were named $G_{1.0}$-EW, $G_{2.5}$-EW, $G_{5.0}$-EW, and $G_{7.5}$-EW and stored in the dark.

2.2.4. Bioink Preparation. The photoinitiator Irgacure 2959 (0.1 g) was accurately weighed and dissolved in 10 mL of phosphate-buffered saline (PBS). Then, 5.0, 4.5, 3.75, or 2.5 g of G-EW($G_{2.5}$-EW) and 0, 0.5, 1.25, or 2.5 g of G-SF, respectively, were added in sequence and stirred until they dissolved. PBS was added dropwise to the mixture to increase the volume to 20 mL, which yielded the final concentration of the photoinitiator Irgacure 2959 (I2959) of 5% (w/v). Three composite bioinks were formulated into 25% (w/v) and named G-EW, G-EW/SF (10%), G-EW/SF (25%), and G-EW/SF (50%).

2.2.5. 3D Printing. The composite bioinks mentioned above were loaded into the injection syringe of the Allevi 1 Printer to prepare porous biological scaffolds. The inks were extruded through a 27 G blunt needle. Printed materials were dispensed onto a glass substrate with a gap size of 2 cm at a speed of 10 mm s^{-1}. The wavelength of ultraviolet light that initiates the cross-linking reaction is 365 nm, and the printer parameters are set to a temperature of 20 °C and a pressure of 10 psi. Construct designs were made by using AutoCAD 2016.

2.3. Physical Performance Test Methods. *2.3.1. Mechanical Properties.* The 3D-printed biological scaffolds were all cylindrical scaffolds with a diameter of 12 mm and a height of 8 mm. The room temperature was around 25 °C, and an electronic tensile testing machine (WH-5000, Ningbo Weiheng Testing Instrument Co., Ltd.) was used to determine the compression performance of the biological scaffold. When the stress−strain curve began to drop sharply, the experiment stopped and the data were recorded. The sample compression test parameters were set as follows: the compression speed is 5 mm/min, n = 3. The slope of the initial linear phase of the stress−strain curve was recorded as the compressive modulus of the biological scaffold. The stress and strain were calculated as the following equation:

$$\text{stress} = F/A$$

where F is the applied force and A is the contact surface area.

$$\text{strain}\ (\%) = H_1/H_2 \times 100$$

where H_1 is the shape variable and H_2 is the original height of sample.

2.3.2. Swelling Ratio Determination. This experiment uses the G-EW/SF composite ink to bioprint various biological scaffolds. The 3D-printed biological scaffolds are cylindrical scaffolds with diameters of 12 mm and heights of 8 mm. Put each group of biological scaffolds into a drying box, dry at 37 °C overnight, and record the weight as M_0. Next, the dried bioscaffold was immersed in a centrifuge tube containing excess PBS, and it was placed in a 37 °C biochemical incubator to absorb water and swell. It was then taken out every 1 h, water on the surface of the sample was wiped off with filter paper, and weighed and recorded as M_n. The sample swelling ratio was obtained according to the formula, n = 3.

$$\text{swelling ratio}\ (\%) = M_n/M_0 \times 100\%$$

2.3.3. Scanning Electron Microscopy (SEM). The biological scaffolds that reached swelling equilibrium in water were frozen at −80 °C and freeze-dried. A flake-shaped sample of the scaffold was sprayed with gold on the surface for 70 s, and the surface and cross section of the sample were observed using an SEM (Regulus 8230, Hitachi, Japan). The SEM acceleration voltage was 15 kV.

2.3.4. Measuring Method of Average Pore Size and Porosity. ImageJ software was used to measure the diameter of 20−50 micropores in the scanning electron micrographs of each group of biological scaffolds to obtain the average pore diameter. The specific porosity was calculated by liquid displacement method described in the author's recent articles.[26]

2.4. Structural Analysis Methods. Fourier transform infrared (FTIR) spectroscopy, X-ray diffraction analysis, and thermal analysis were conducted according to the method recently reported by the author.[29] Fourier transform infrared spectrometer (Nicolet 6700, Thermo Fisher) was used to detect the molecular structure characteristics of SF, EW, and each group of biological scaffolds, and potassium bromide crystals were mixed with the above-mentioned sample powder to be tested and ground. Take a small amount of mixed sample powder, press it into flakes, and start the test. The test parameters are set as follows: the number of scans is 16, the resolution is 4 cm^{-1}, and the spectral range is 2000−1000 cm^{-1}. The sample powders were analyzed by using an X-ray diffractometer (D8 Advance, Bruker, Germany). The test parameters were set as copper target, tube voltage 40 kV, tube flow 40 mA, wavelength 0.15 nm, diffraction angle 2θ range from 5 to 50°, scanning step size 0.03°/step, scanning speed 12.5°/min. Thermogravimetry (TG) was measured with a thermogravimetric/differential thermal analyzer (SDT2960, TA), and the data were processed by derivation to draw a derivative thermogravimetry (DTG) curve. The test parameters are set as nitrogen protection, temperature range 25−800 °C, and heating rate 10 °C/min.

2.5. *In Vitro* Degradation and Release Experimental Methods. The neutral protease degradation rate and insulin sustained release rate were measured and calculated according to the method recently reported by the author.[30] The mixed bioink was injected into the syringe barrel of the Allevi 1 printer to form a cylindrical porous bioscaffold with a diameter of 12 mm and a height of 8 mm. The neutral protease was prepared as a solution of 10 U/mL so that the dry weight of the bioscaffold to the mass-volume ratio of the added protease solution was 50 mg/mL. PBS was used to dissolve bovine insulin in a drug sustained release to obtain 27 U/L insulin solution. The prepared insulin solution was mixed with each group of bioinks at a volume ratio of 1:9 for 3D printing.

2.6. Cell Culture. In this experiment, mouse fibroblast cells L-929 were used for a cytocompatibility test to detect the viability of cells growing on biological scaffolds. The medium is DMEM high-glucose medium containing 10% fetal bovine serum and 1% penicillin. The cell incubator parameters were set to a temperature of 37 °C and a CO_2 concentration of 5%; the specific cell culture steps, cell plating, cell morphology observation, and cell viability detection methods were conducted following the methods recently reported by the author.[26] The composite bioink was injected into the syringe barrel of the Allevi 1 printer to make a disc-shaped porous bioscaffold with a diameter of 12 mm and a height of 1 mm, which was placed in a 48-well plate. The density of cell seeding was 500 μL of cell suspension with a density of 10^4/mL for each sample. The cells were stained with calcein AM and propidium iodide (PI) reagents and were photographed under

https://doi.org/10.1021/acsomega.3c05810
ACS Omega 2023, 8, 46685−46696

an inverted fluorescence microscope. During the culture period, the 48-well plate was taken out of the incubator every day, and the cell growth status was observed and recorded under an inverted fluorescence microscope. At the same time, the cells were fluorescently stained. In order to study the effect of printing composite ink on the viability of L-929 cells, CCK-8 was used to measure the cell viability of various bioscaffolds every day and the OD value of each well at a wavelength of 450 nm was detected.

2.7. Data Analysis. The experimental data were calculated by Origin 10.0 statistical software. The results are presented as mean ± standard deviation (SD). Statistical analysis for experimental data was carried out using a one-way analysis of variance (ANOVA) analysis. A p-value < 0.05 was considered to be significant.

3. EXPERIMENTAL RESULTS

3.1. Composite Bioink. *3.1.1. 3D Printing.* The EW, SF, or EW/SF composite scaffolds prepared by 3D printing of the bioinks or composite bioinks are shown in Figure 2. The

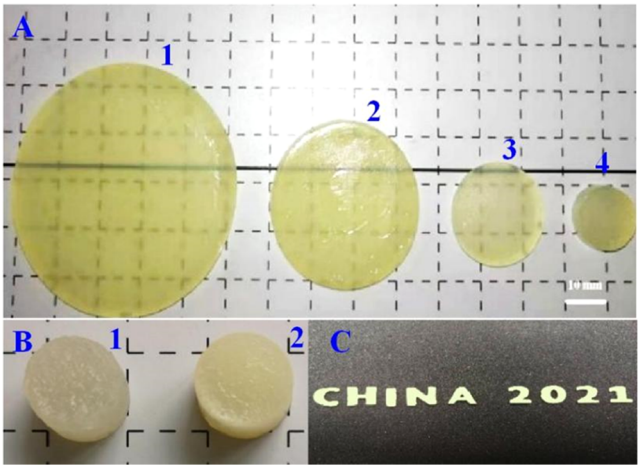

Figure 2. EW/SF 3D composite scaffold based on the G-EW/SF ink. (A1−A4) Composition of the EW/SF composite biological scaffold given in Table 1. (B1, B2) SF scaffold and EW scaffold based on G-SF ink and G-EW ink, respectively. (C) EW/SF (25%) scaffolds based on G-EW/SF (25%) ink. The wavelength of UV light that initiates the cross-linking reaction is 365 nm, and the printer parameters are set as temperature 20 °C and pressure 10 psi.

bioscaffolds based on G-EW alone, G-SF alone, and G-EW/SF inks were printed into various shapes including a disk, column, and other shapes. The EW-based biological scaffold is translucent, soft, and elastic. Therefore, the biological scaffolds based on EW and SF have shape plasticity and can be adapted to different medical application scenarios.

3.1.2. Synthesis of Bioink. The G-EW and G-EW/SF composite inks prepared with G-EW and G-SF in specific ratios are reported in Figure 3 and Table 1. The pure G-EW bioink is light yellow. As G-SF is mixed with G-EW($G_{2.5}$-EW) in mass ratios of 10, 25, and 50%, the color of the composite ink darkens slightly with additional G-SF, but it is not very obvious. In general, these four bioinks are creamy yellow.

3.2. Mechanical Properties. *3.2.1. Influence of GMA Content on the Mechanical Properties of the Pure EW Scaffold.* The protein composition of EW includes ovalbumin, ovotransferrin, and ovomucoid. The side chains of these proteins contain a large number of $-NH_2$ and $-COOH$

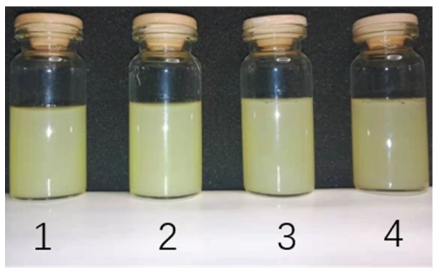

Figure 3. G-EW and G-EW/SF composite inks were prepared with G-EW and G-SF in different proportions. From left to right in the figure are G-EW and G-EW/SF ink. The numbers are 1, 2, 3, and 4 in Table 1, which gives the specific compositions of the G-EW-SF bioinks prepared.

Table 1. Composition of G-EW and G-EW/SF Bioinks (20 mL)

no.	composite bioink	G-SF (g)	G-EW (g)	photoinitiator (g)
1	G-EW		5.00	0.10
2	G-EW/SF (10%)	0.50	4.50	0.10
3	G-EW/SF (25%)	1.25	3.75	0.10
4	G-EW/SF (50%)	2.50	2.50	0.10

groups, facilitating the chemical cross-linking of the EW to form a gel. In this experiment, glycidyl methacrylate was used for the first time to replace the free amino groups in the EW, and the EWs were grafted and modified. In the presence of a photoinitiator, the modified EW can be polymerized by ultraviolet light to initiate free radical polymerization and form a biological protein scaffold with a certain mechanical strength. GMA (1.0 2.5, 5.0, and 7.5 mL) was slowly added to 100 mL of homogeneous EW solution (10%, w/v). Then, the mechanical properties of the obtained G-EW biological scaffolds were measured. For the analysis of compressive strength of different SF-based inks, refer to the article recently reported by the author.[26]

As shown in Figure 4a, the stress of the $G_{1.0}$-EW biological scaffold at 70% strain is 0.107 MPa, the maximum compressive strain of the $G_{2.5}$-EW biological scaffold is 75%, and the compressive stress at fracture is 0.208 MPa. The maximum compressive strains of the $G_{5.0}$-EW and $G_{7.5}$-EW biological scaffolds are 46 and 47%, respectively, much lower than the maximum compressive strains of the $G_{2.5}$-EW biological scaffold, and the compressive stress at fracture are 0.142 and 0.132 MPa, respectively. As shown in Figure 4b, the compressive modulus of the $G_{2.5}$-EW biological scaffold is about 0.012 MPa, which is slightly higher than that of the $G_{1.0}$-EW biological scaffold but much lower than that of the $G_{5.0}$-EW and $G_{7.5}$-EW scaffolds. As the amount of added GMA increases, the compressive modulus of the EW biological scaffold also increases. However, $G_{5.0}$-EW and $G_{7.5}$-EW are difficult to dissolve, and there are many substances similar to precipitation. The excessive amount of GMA likely causes excessive cross-linking of the EW in these samples. Therefore, in the following experiments, 2.5% (v/v) GMA was selected for the grafting of EW. In addition, the compressive strength of the different SF-based inks was also described and analyzed in the results recently published by the authors.[26]

3.2.2. Effect of G-SF Level on the Mechanical Properties. In order to improve the properties of EW biological scaffolds, grafted SF was incorporated into EW/SF composite scaffolds at mass ratios of 10, 25, and 50%, and the mechanical

https://doi.org/10.1021/acsomega.3c05810
ACS Omega 2023, 8, 46685−46696

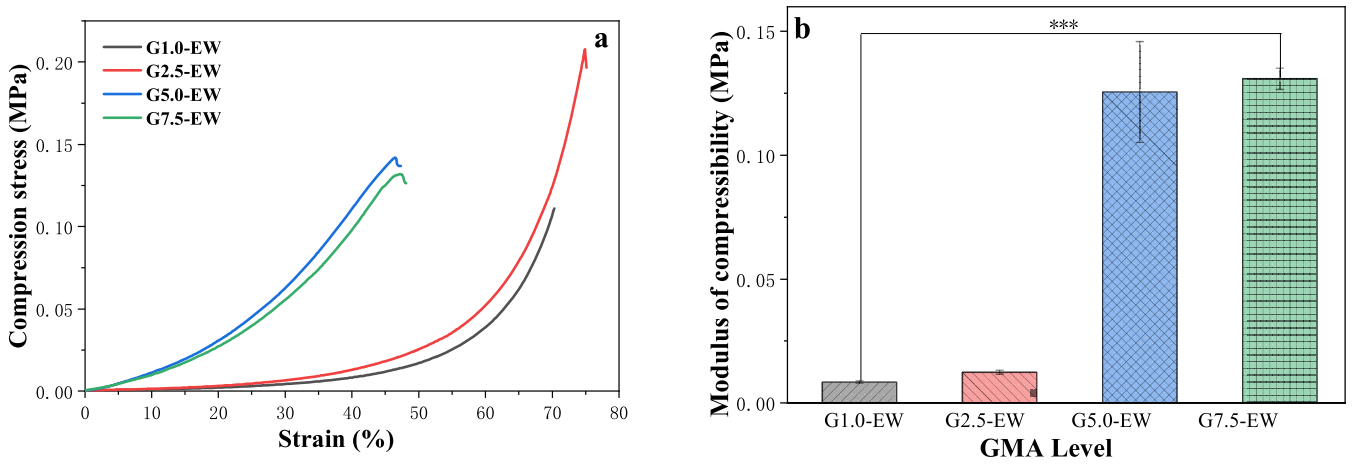

Figure 4. Effect of added GMA on the mechanical properties of the EW biological scaffold. (a) Stress−strain curve and (b) compressive modulus of the EW biological scaffold; *** indicates $P < 0.001$, and the difference is extremely significant.

properties of these EW/SF composite biological scaffolds were determined. As shown in Table 2, with increased G-SF content, the mechanical properties of the EW/SF composite scaffold change compared with the pure EW scaffold. The compressive strength and compressive modulus increase to varying degrees, but the maximum compressive strain trends downward. The compressive strength of the pure EW scaffold ranges from 0.207 to 0.263 MPa, and the compressive modulus is around 0.012 MPa. While the compressive strength of the EW/SF (50%) composite scaffold ranges from 0.257 to 0.307 MPa, the compression modulus is about 0.061 MPa, which is almost 5 times higher than that of the pure EW scaffold. This difference shows that increasing the content of G-SF can significantly improve the mechanical properties of the EW/SF composite biological scaffold and overcome the insufficient strength of the EW material that results from the molecular structure of the globular protein.

Table 2. Mechanical Properties of EW/SF Composite Scaffolds[a]

3D scaffolds	compressive strength (MPa)	max compressive strain (%)	compressive modulus (MPa)
EW alone	0.235 ± 0.028	77.436 ± 2.511	0.012 ± 0.001
EW/SF (10%)	0.250 ± 0.041	80.391 ± 3.084	0.018 ± 0.003*
EW/SF (25%)	0.252 ± 0.028	77.805 ± 2.633	0.021 ± 0.004*
EW/SF (50%)	0.282 ± 0.025	73.473 ± 3.157	0.061 ± 0.002***

[a]The data in the table are mean ± SD, $n = 3$; * indicates the difference compared with the pure EW scaffold; * indicates $P < 0.001$, the difference is extremely significant.

3.3. Microstructure. In this experiment, ImageJ software was used to determine the internal pore size distribution of the synthetic scaffold, and the porosity of each group of freeze-dried biological scaffolds was measured by the liquid displacement method. Figure 5 shows that all of the bioscaffolds have a good porous network structure, which guarantees cell adhesion and migration. The average pore size of the pure EW scaffold is only 30 ± 10 μm, while the average pore sizes of the EW/SF composite bioscaffolds prepared by incorporating G-SF at mass ratios of 10, 25, and 50% are about 41, 44, and 61 μm, respectively. The incorporation of G-SF can significantly increase the average pore size of the EW/SF composite scaffold. The ideal pore size of a porous scaffold used for skin tissue repair is 20−125 μm. Therefore, each of these biological scaffolds meets the cell growth pore size requirements for skin tissue repair.

The average pore sizes and porosities of various scaffolds are given in Figure 6. The average pore size for all of the samples is 20−50 μm. The pore size of the scaffolds increases significantly as the proportion of G-SF increases. The porosity of the pure EW scaffold is 70%, and the porosity of the EW/SF composite scaffold modified with 10, 25, and 50% mass ratio of grafted SF is about 74, 78, and 82%, respectively. The experimental results show that the porosity of the modified EW/SF composite scaffold increases with the incorporation of G-SF, yielding porous structures with larger pores. Such a porous biological scaffold is very suitable for cell growth and facilitates the exchange of nutrients between the cells and the extracellular environment.

3.4. Fourier Transform Infrared (FTIR) Spectroscopy. The structural differences of SF and EW and the composite biological scaffolds were analyzed by Fourier transform infrared spectroscopy, and the results are shown in Figure 7. Polypeptide and protein repeat units can produce multiple characteristic infrared absorption peaks, including amides I, II, and III. Amide I is in the range 1600−1690 cm^{-1} and derives from the C═O bond stretching vibration. Amide II is in the range of 1480−1575 cm^{-1}, derived from the bending vibration of the NH bond and the stretching vibration of the CN bond. Amide III in the range of 1229−1301 cm^{-1} is mainly caused by the bending vibration of the NH bond and the stretching vibration of the CN bond.[31] In the infrared spectrum of the bracket after GMA grafting, some feature bands are reflected in each group: a methyl acylhlitol group at 1700 cm^{-1} causes the extension of C═O, due to the ethylene group at 1637 cm^{-1} caused the extension of C═C, the breathing of the epoxy resin ring at 1255 cm^{-1}. The molecular weight of the GMA is much smaller than that of EW and SF, so the GMA's functional group can only be slightly tested or hidden by the EW peak.[31] FTIR comparison of SF and SF-GMA was described in the recent article reported by the author.[26]

As shown in Figure 7, EW powder, the pure EW scaffold, and the EW/SF (50%) composite scaffold have two distinct characteristic peaks between 2000 and 1000 cm^{-1}. The first characteristic peak is at about 1650 cm^{-1}; the absorption peaks

https://doi.org/10.1021/acsomega.3c05810
ACS Omega 2023, 8, 46685−46696

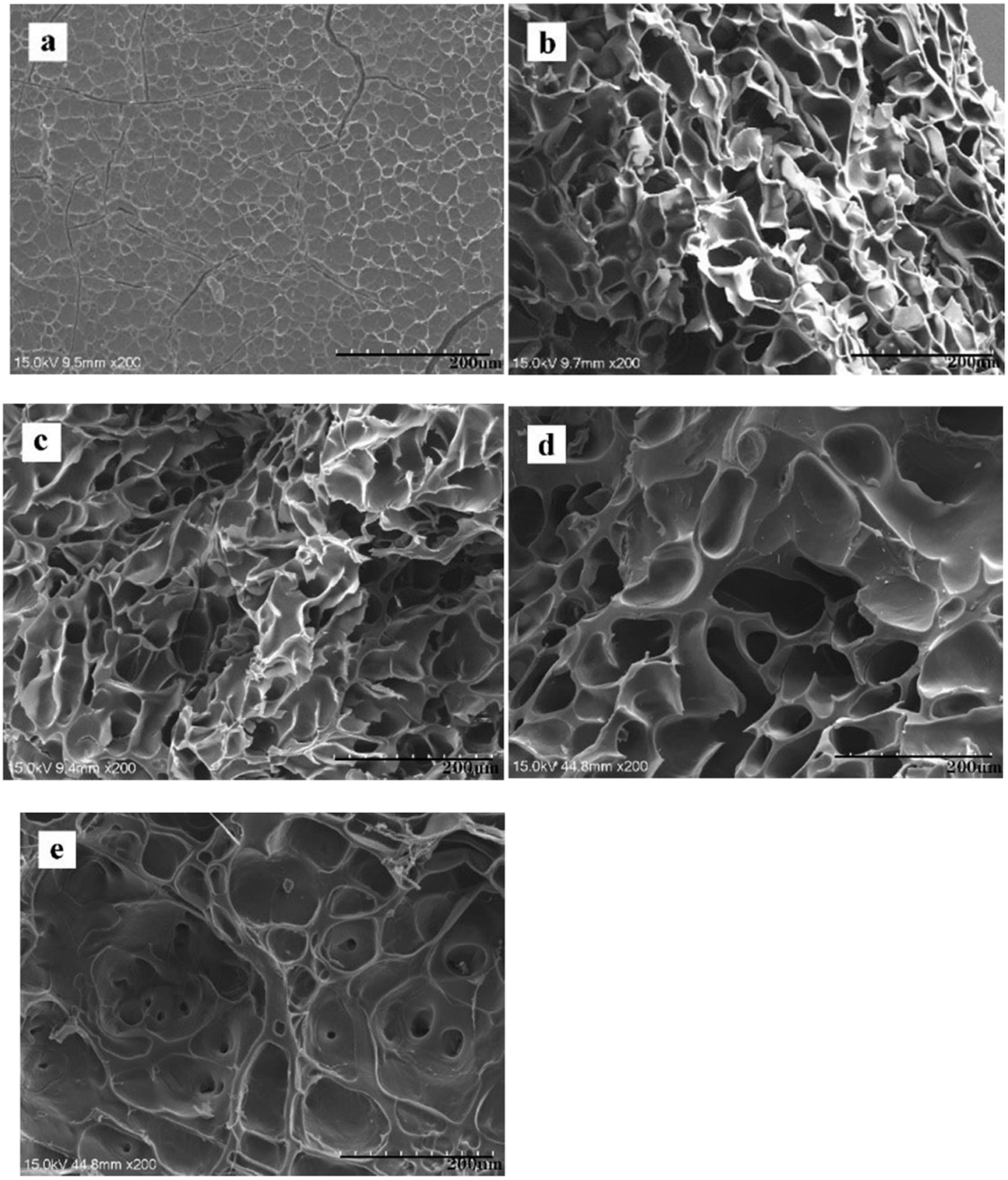

Figure 5. Microstructure of the surface and cross section of the biological scaffolds (×200). (a) Surface structure of a pure EW scaffold; cross-sectional structure of (b) EW, (c) EW/SF (10%), (d) EW/SF (25%), and (e) EW/SF (50%) scaffolds; scale bars are all 200 μm.

of α-helix and random coils of amide I are in the range of 1650−1658 and 1640−1648 cm^{-1}, respectively, indicating that the protein secondary structures of EW powder, pure EW scaffold, and EW/SF (50%) composite scaffold includes the random coil and α-helix structures. The second peak of the EW powder is located at 1539 cm^{-1}, which belongs to the random coil structure. The second peak in the EW and EW/SF (50%) biological scaffolds is at about 1515 cm^{-1}, which belongs to the β-sheet structure. This difference shows that EW, like SF, undergoes a rearrangement of its structure after being grafted and solidified into a biological scaffold, changing from random crimping to a β-sheet structure. The characteristic peak of the EW/SF (50%) bioscaffold is sharper at 1515 cm^{-1}, indicating that the interaction between the G-EW and G-SF may be due to enhanced crystallization. In addition, the EW powder, pure EW scaffold, and EW/SF (50%) composite scaffold all have a small peak at about 1235 cm^{-1}, which belongs to the random coil structure in amide III.

3.5. X-ray Diffraction. As shown in Figure 8, the EW powder, EW scaffold, and EW/SF (50%) composite scaffold all have an obvious characteristic peak at $2\theta = 20°$. Moreover, compared with the EW and EW/SF (50%) bioscaffolds, the EW powder has a broader peak at $2\theta = 20°$, indicating that the amount of β-sheet structure significantly increases after the EW is solidified into a bioscaffold. This result is also consistent with FTIR spectroscopy analysis.

3.6. Thermal Analysis. The TG curves of the pure EW scaffold and EW/SF composite biological scaffold are shown in

https://doi.org/10.1021/acsomega.3c05810
ACS Omega 2023, 8, 46685−46696

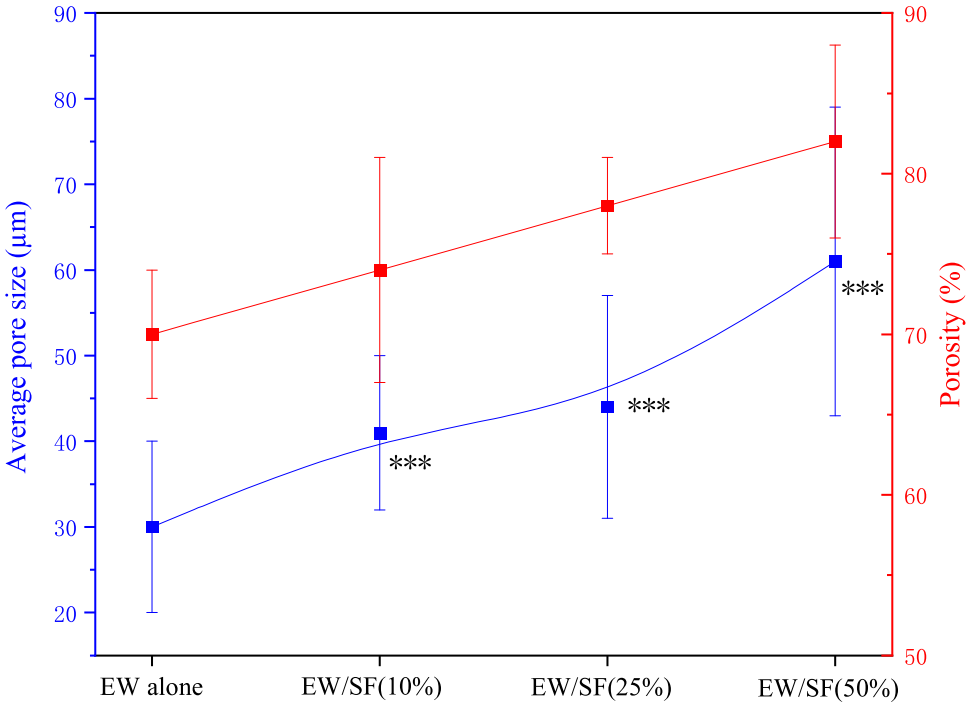

Figure 6. Average pore sizes and porosity of EW alone and EW/SF composite scaffolds; * indicates the difference between the EW/SF composite bioscaffold and the pure EW scaffold; *** indicates $P < 0.001$, the difference is extremely significant, $n = 3$.

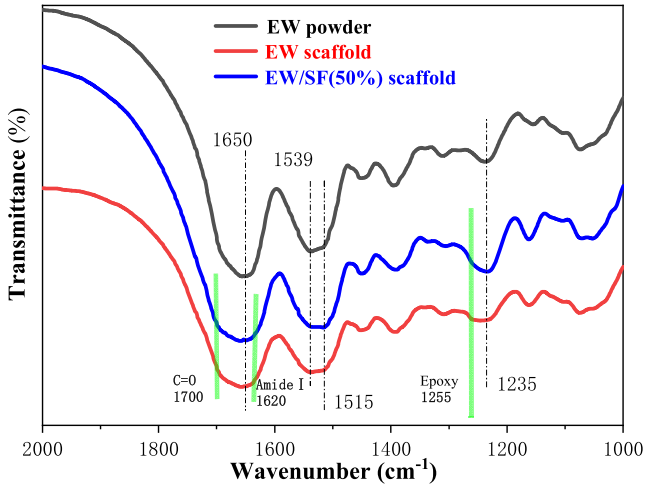

Figure 7. FTIR spectra of the EW powder, the pure EW scaffold, and the EW/SF (50%) scaffold.

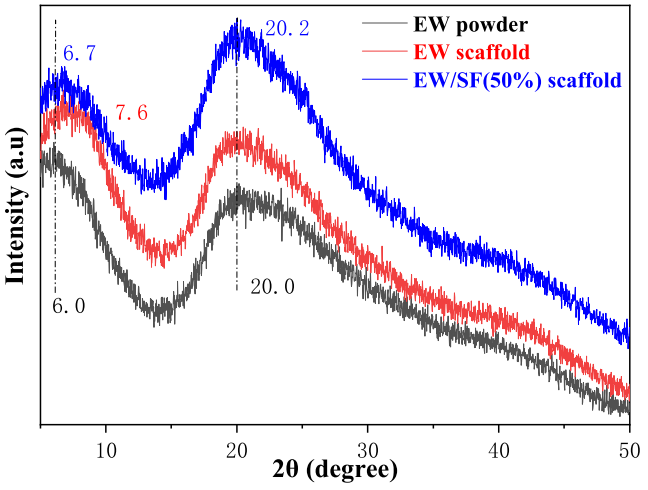

Figure 8. X-ray diffraction spectra of the EW powder, the pure EW scaffold, and the EW/SF (50%) scaffold.

Figure 9a and can be divided into four stages. First, the EW powder has an initial weight loss below 90 °C, while the EW and EW/SF (50%) scaffolds have an initial weight loss below 120 °C. When the EW powder is between 90 and 230 °C, and the EW and EW/SF (50%) biological scaffolds are between 120 and 230 °C, they have low mass loss, which is the second stage. In the third stage, the decomposition rate of the EW powder, pure EW scaffold, and EW/SF (50%) composite biological scaffold rapidly accelerates between 230 and 430 °C. The mass of the EW and EW/SF composite biological scaffolds gradually stabilizes after 430 °C, which is the fourth stage.

Figure 9b shows that the weight loss rate of the EW powder, the pure EW scaffold, and the EW/SF (50%) composite biological scaffold is greatest at 301, 312, and 307 °C, respectively. At this time, the peptide bonds within the SF protein and the EW molecules are broken. The C−N bond, which has a lower bond energy, is rapidly broken, and the C−C, C═O, and N−N bonds will also be broken. In addition, the thermal decomposition temperature of the EW biological scaffold is 10 °C higher than that of the EW powder. These results indicate that added GMA significantly improves the thermal stability of the EW/SF composite scaffold.

3.7. Swelling Ratio. The swelling performance of the biological scaffold is a very important parameter that evaluates the water absorption capacity. The swelling capacity of a bioscaffold is determined by its porous structure and the presence of hydrophilic groups. As shown in Figure 10, the swelling ratio of the EW/SF composite scaffold continuously increases within the first 12 h. The swelling ratios of the pure

https://doi.org/10.1021/acsomega.3c05810
ACS Omega 2023, 8, 46685−46696

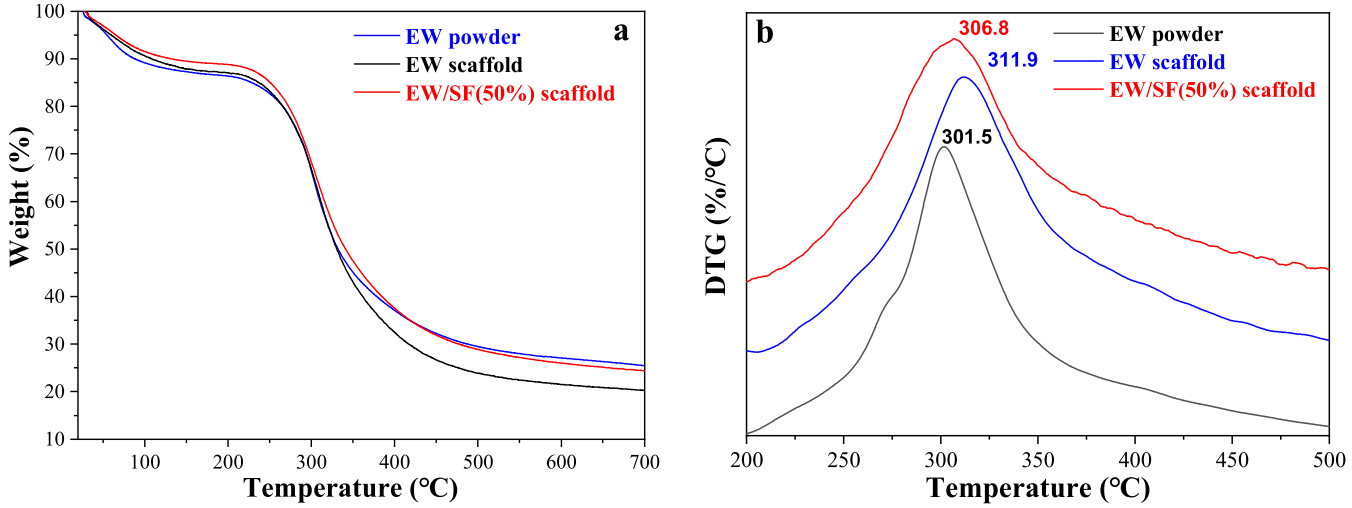

Figure 9. (a) TG and (b) DTG thermal analysis spectra of the EW powder, pure EW scaffold, and EW/SF (50%) composite scaffold.

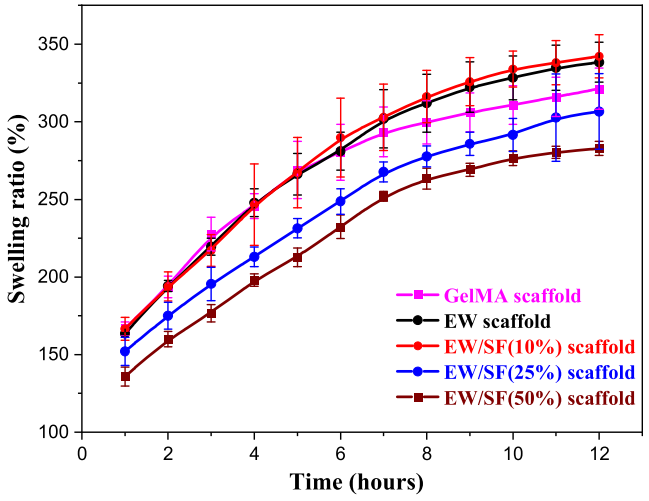

Figure 10. Swelling behavior of the EW scaffold and three EW/SF composite scaffolds. The preparation method of the gelatin (GelMA) scaffold as a control sample refers to the method reported in the author's just published paper.[26] $n = 3$.

EW scaffold and the EW/SF (10%) bioscaffold increase from the seventh hour. Both ratios are consistently higher than the swelling ratios of the EW/SF (25%) and EW/SF (50%) biological scaffolds for the entire period, and the swelling ratio of the first two samples [pure EW scaffold and the EW/SF (10%)] is about 340% after 12 h, while the latter two [EW/SF (25%) and EW/SF (50%)] are, respectively, 310 and 280%. It is known that the swelling ratio of GMA-SF alone was only about 254% after swelling for 12 h in the article reported recently by the author.[26] It can also be observed from the figure that the swelling ratio of the EW scaffold and the EW/SF (10%) containing the low content of silk fibroin after 12 h is higher than that of the control sample gelatin scaffold, while the swelling ratio of the EW/SF scaffolds with high content of silk fibroin will be lower than that of the control sample. The addition of modified SF reduces the swelling performance of the EW/SF composite scaffold to a certain extent, and as the proportion of G-SF increases, the swelling ratio of the biological scaffold lowers. Therefore, the swelling capability of the EW/SF composite scaffold can be adjusted by adding G-SF.

3.8. Enzymatic Degradation. The enzymatic degradation curve of the EW/SF composite scaffold is shown in Figure 11. The mass remaining of the pure EW bioscaffold with G-EW enzyme degradation after 9 days is about 10%, and the addition of G-SF can significantly delay the degradation of the EW/SF composite bioscaffold. Among the composite bioscaffolds, the mass remaining of the EW/SF (50%) bioscaffold after 9 days of degradation is about 28%, which is nearly 18% higher than that of the EW scaffold. The degradation rate of the EW/SF composite bioscaffold is lower than that of the EW bioscaffold. This effect may be because the SF scaffold has a higher mass remaining after degradation, and the copolymerization of G-EW and G-SF forms a porous structure, which prevents the rapid degradation of the EW in the EW/SF composite bioscaffold. The results show that the mass residual ratios of these four EW alone and EW/SF bioscaffolds are still lower than that of the control GelMA scaffold based on commercialized gelatin bioink; the EW bioscaffold is easily degraded, but adding G-SF to EW forms a porous structure that reduces the degradation rate. Therefore, G-SF can be used to adjust the degradation performance of the bioscaffold, which is conducive to the growth of new tissues and sustained release of embedded drugs.

3.9. Drug Sustained Release Ability. The porous structure of the biological scaffolds can be loaded with drugs, which prolongs the retention time in the body, thereby improving the medicinal effect. The insulin release curves of the EW/SF composite biological scaffolds are shown in Figure 12. The insulin release rate of the EW alone scaffold and the EW/SF (10%) composite biological scaffold is approximately 10% on day 1, the difference is very significant compared to the control GelMA scaffold. With the extended release times, the insulin release ratios of the EW alone biological scaffolds and EW/SF (10%), EW/SF (25%), and EW/SF (50%) composite biological scaffolds gradually increase, and the release rate after 3 days all exceeded the control; the release rates after 5 days are approximately 78, 80, 73, and 70%, respectively. Among them, the release rate of the EW/SF (10%) bioscaffold on day 5 is very significant. The addition of 10% G-SF can improve the sustained release ability of the EW/SF composite scaffold. However, it is not clear why the drug release in the first 3 days increases with the addition of G-SF, but the drug release in the fifth day is not high.

https://doi.org/10.1021/acsomega.3c05810
ACS Omega 2023, 8, 46685−46696

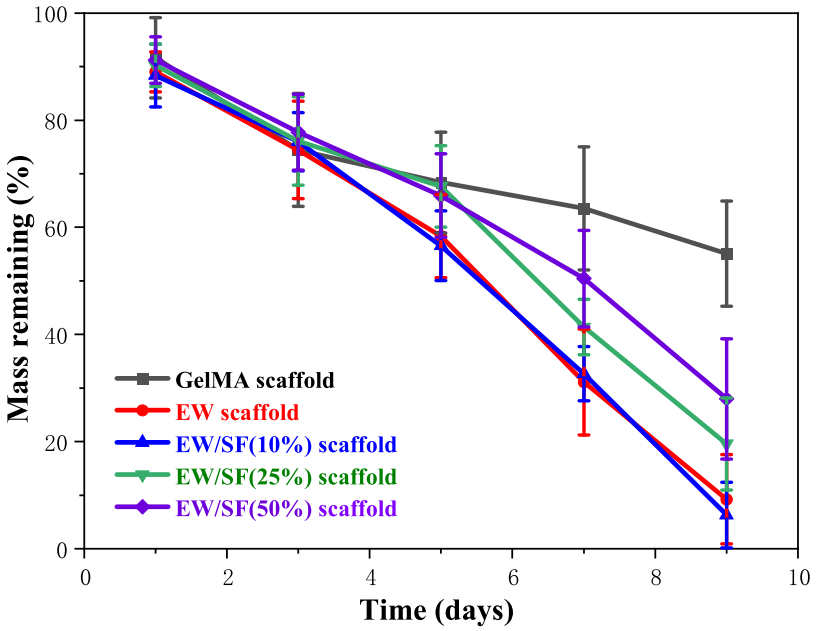

Figure 11. Effect of neutral protease on the *in vitro* degradation of pure EW scaffold, GelMA scaffold, and three EW/SF composite scaffolds. $n = 3$, $^{\#}$ $p < 0.05$, versus EW scaffold group.

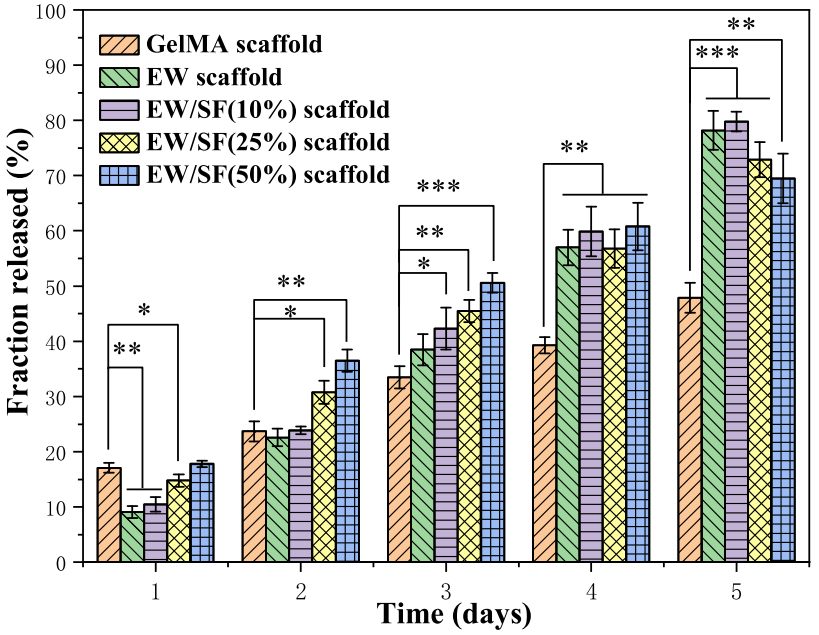

Figure 12. Bovine insulin release profile of the pure EW scaffold and the three EW/SF composite scaffolds. $n = 3$, * indicates the difference compared with the EW alone biological scaffold control group, * indicates $P < 0.05$, the difference is significant; ** means $P < 0.01$, the difference is very significant; *** means $P < 0.001$, the difference is very significant.

3.10. Cell Compatibility. Cell compatibility is an important parameter for the evaluation of biomedical materials. The cell compatibility of the bioscaffold mainly depends on its influence on cell behavior. The L-929 mouse fibroblast was used as the model cell for this experiment. It was inoculated on the surface of aseptically treated pure EW scaffold and three EW/SF composite scaffolds at the same cell density for culturing, and the growth status of the cells was regularly observed and recorded. The cell viability of L-929 on various biological scaffolds was measured on days 1, 2, 3, and 4. The results are shown in Figure 13.

On the fourth day of cell seeding, the growth status of L-929 was observed under normal light. One day after the cells were seeded on the surface of the biological scaffold, most of them were circular, sparse, and evenly distributed on the surface of the biological scaffold, and they all gradually adhered to the surface of the biological scaffold. The cell shape changed from a spherical shape to a spindle shape. In order to observe the changes of cell growth morphology more clearly, eliminate background influence, and distinguish living and dead cells, we fluorescently stained L-929 with Calcein AM and propidium iodide (PI). As shown in Figure 13a–d, on the fourth day, the cells survived in large numbers on the surface of the biological

https://doi.org/10.1021/acsomega.3c05810
ACS Omega 2023, 8, 46685−46696

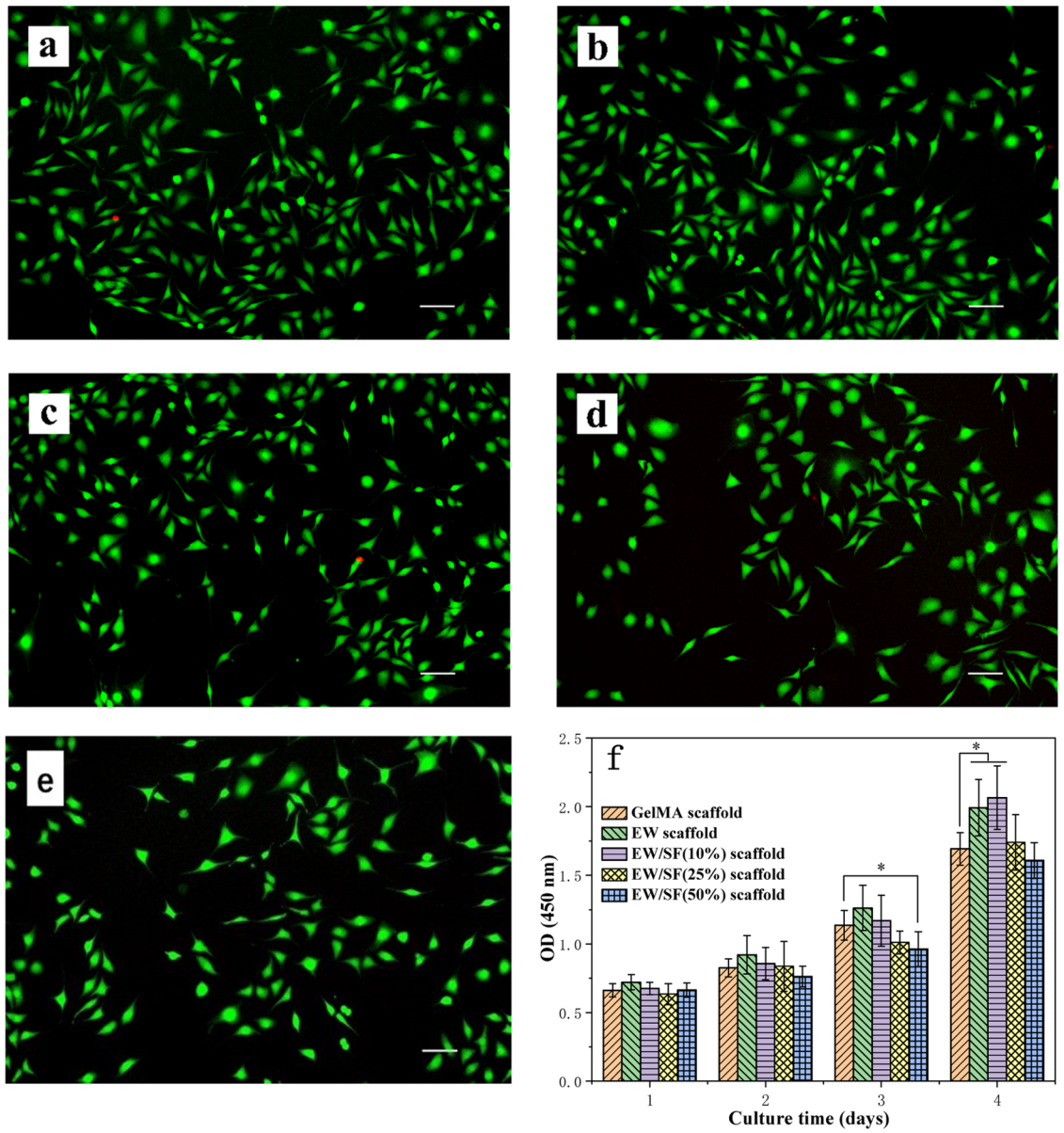

Figure 13. Microscopic pictures and cell viability of mouse fibroblasts L-929 on the pure EW scaffolds and three EW/SF composite scaffolds. Photomicrographs of (a) L-929 cells grown on the pure EW scaffold, (b) EW/SF (10%), (c) EW/SF (25%), and (d) EW/SF (50%) composite scaffolds on day 4 (fluorescence 200×); (e) L-929 cells grown on GelMA scaffold; (f) the growth curve of L-929 on the above four types of scaffolds; the scales in the figure are all 200 μm; n = 5, * indicates the difference compared with the EW alone bioscaffold as control group, * indicates $P < 0.05$, the difference is significant.

scaffold, and almost all of them had a spindle shape and were densely distributed on the surface of the biological scaffold. The pseudopodia of the cells stretched longer, and most of them showed a mature spindle shape. The cells grew vigorously, while the dead cells (red in Figure 13) were scarce. Both the pure EW biological scaffold and the EW/SF composite biological scaffold support the adhesion, as shown in Figure 13a−d of L-929, and obvious differences between the four were not distinguished.

In order to further evaluate the effect of the printing composite ink on cell growth, the CCK-8 method was used to determine the cell viability on each scaffold every day. As shown in Figure 13f, although there was no significant difference between the egg white/silk fibroin composite bioscaffold in the early stage and the control, the GMA-EW/SF (50%) bioscaffold, GMA-EW pure egg white bioscaffold and GMA-EW/SF (10%) on day 3 The OD_{450} values of the bioscaffolds on day 4 were significantly different from those of the control GelMA scaffold. It can be seen that egg whites can significantly improve the cell viability of L-929. Among them, the EW-10% SF composite scaffold not only has excellent compatibility with L-929 cells but also possesses the mechanical properties discussed earlier, making it a potential cell culture substrate for intensive research.

4. DISCUSSION

EW is rich in sources and low in cost. The development and utilization of medical biomaterials have just started, and there are few reports in the field of bioink application research. SF has good biocompatibility and degradability, and EW has excellent biological properties, such as antioxidant, anti-inflammatory, and antibacterial. The use of SF and EW to

https://doi.org/10.1021/acsomega.3c05810
ACS Omega 2023, 8, 46685−46696

develop new bioinks, explore the utilization value of EW, develop medical biomaterials based on SF and EW, and expand their applications in the fields of biomedicine and tissue engineering, which have long-term practical significance and broad application prospects. The EW/SF composite bioscaffold prepared in this experiment has certain mechanical properties and porous network structure, which is conducive to the transport of biological active substances and the discharge of cell metabolites and improves the adhesion and growth of cells, thus meeting the requirements for medical tissue engineering applications condition.

After being implanted in the body, bioscaffolds printed or prepared by mixing EW with other polymers or inorganic substances will show high antioxidant activity as the degradation continues, but its mechanical properties are still its weakness and that the degradation rate is difficult to control. It has been reported that a composite bioink composed of sodium alginate and EW was 3D-printed as a scaffold for tissue engineering. It has good biocompatibility, the maximum swelling value in the medium was 17.12 ± 0.53%, but has not been tested and analyzed for mechanical properties.[32] It also has been reported that a natural EW gel was successfully fabricated by the 3D direct writing technique, the EW hydrogel was synthesized by mixing with an alkaline solution, and the resulting 3D secondary ionic bond network was achieved through a physical cross-linking strategy. The highest mechanical strength is 17.8 ± 6.2 kPa, and the elongation is about 60%. And so far, there has been no report on the use of covalent bonding of light-curing agents to make EW bioinks. G-EW alone has limitations in its mechanical properties, enzymatic degradation rate, pore size, etc. This experiment mixed G-EW and G-SF to prepare G-EW/SF composite bioinks. The purpose was to improve the mechanical properties and enzymatic degradation rates of the bioscaffolds. The experimental results show that the 3D scaffold printed with the G-EW/SF composite bioink has improved in these two aspects. The maximum compressive strength of G-EW/SF (10%) and G-EW/SF (50%) reaches 0.250 ± 0.041 MPa and 0.282 ± 0.025 MPa, respectively. Structural analysis showed that the β-sheet structure of EW and SF was increased after GMA grafting, so the mechanical properties and thermal stability were also enhanced after graft modification. After the addition of G-SF, the enzymatic hydrolysis rate of the EW/SF composite scaffold also increased and the pore size also became larger, which was more conducive to the growth and proliferation of cells. The compressive strength of the EW composite scaffold with 50% grafted SF is 20% higher than that of the pure EW scaffold and shows a dose effect. The EW composite scaffold has a three-dimensional network structure conducive to cell growth and proliferation, with an average pore size range of 41−61 μm. The more grafted SF that is incorporated, the larger the pore size. The thermal decomposition temperature of the EW/SF composite scaffold is 10 °C higher than that of the EW scaffold alone. The residual ratio of the EW composite scaffold after enzymolysis for 9 days is about 18% higher than that of the pure EW scaffold, and its insulin sustained release performance is significantly improved. *In vitro* culture experiments show that many spindle-shaped L-929 cells can be observed on this EW composite scaffold and the cells have good stretchability, which promotes cell adhesion and proliferation. Therefore, it is a good choice to incorporate SF into the EW bioinks for 3D printing EW/SF composite scaffolds, and it will expand the application of EW in biomedicine and tissue engineering.

5. CONCLUSIONS

Preparing homogenized egg white using the high-speed shearing method overcomes the shortcoming of the difficulty of mixing the concentrated liquid and the thin liquid of the EW. The grafting reaction of the homogenized EW and GMA obtains GMA-modified EW. Silk, which has good mechanical properties, was successfully introduced into EW bioinks to make G-EW/SF composite ink. These G-EW/SF composite inks have a compressive strength of 0.24−0.28 MPa, a maximum compressive strain of 73.47−80.39%, a compressive modulus of 0.01−0.06 MPa, and a swelling ratio of 280−340%. Infrared spectroscopy and X-diffraction detection results showed that EW, like SF, rearranged its structure from a random coil to β-sheet structure after transplantation and curing into bioscaffolds. The thermal analysis results showed that added G-SF significantly improved the thermal stability of the EW/SF composite scaffold. The EW/SF composite scaffold has a porous network structure with a pore size distribution in the range of 40−60 μm. The EW/SF (50%) composite scaffold mixed with 50% G-SF ink has a residue ratio 18% higher than that of the pure EW scaffold after 9 days of hydrolysis with neutral protease. After 5 days, the insulin release rate is reduced by 8%. These EW/SF composite scaffolds with porous networks can fully meet the needs of cell growth and proliferation. In the future, it can be used as a new type of medical biomaterial. For example, they can be used as wound dressings and artificial skin to repair skin tissue.

AUTHOR INFORMATION

Corresponding Author

Yu-Qing Zhang − *School of Biology and Basic Medical Sciences, Medical College, Soochow University, Suzhou 215006, P. R. China;* orcid.org/0000-0001-7670-386X; Email: sericult@suda.edu.cn

Authors

Hai-Yan Wang − *Stomatology Department, The People's Hospital of Suzhou New District, Suzhou 215000, P. R. China*

Shu-Xiang Zhao − *School of Biology and Basic Medical Sciences, Medical College, Soochow University, Suzhou 215006, P. R. China*

Ji-Xin Li − *School of Biology and Basic Medical Sciences, Medical College, Soochow University, Suzhou 215006, P. R. China*

Complete contact information is available at: https://pubs.acs.org/10.1021/acsomega.3c05810

Author Contributions

§H.-Y.W. and S.-X.Z. contributed equally to this study.

Author Contributions

This article is an original research work. All authors have seen the manuscript and approved to submit to your journal. This paper has not been previously published to any other journal, and will not be submitted elsewhere before a decision is made by this journal. We would be glad if our manuscript would give you desired excellence. Thank you very much for your attention and consideration.

https://doi.org/10.1021/acsomega.3c05810
ACS Omega 2023, 8, 46685−46696

Notes

The authors declare no competing financial interest.

■ ACKNOWLEDGMENTS

This study was funded by the China Agriculture Research System (CARS-18-ZJ0502), the Priority Academic Program Development of Jiangsu Higher Education Institutions (PAPD), the Medical Education Collaborative Innovation Fund of Jiangsu University (JDYY2023127), the Science and Innovation Project funded by The People's Hospital of Suzhou New District (SGY2020E02), the Science and Technology development of Suzhou Science and Technology Bureau (SKJYD2021059 and SKYD2022091), and the Medical and Health Youth Science and Technology Project funded by Suzhou New District (2020Q008).

■ REFERENCES

(1) DeSimone, E.; Schacht, K.; Pellert, A.; Scheibel, T. Recombinant spider silk-based bioinks. *Biofabrication* **2017**, *9* (4), No. 044104.
(2) Chen, L.; Powrie, W. D.; Nakai, S. *The Chemistry of Eggs and Egg Products in Egg Science and Technology*, 4th ed.; CRC Press, 2017; pp 101−172.
(3) Babaei, J.; Mohammadian, M.; Madadlou, A. Gelatin as texture modifier and porogen in egg white hydrogel. *Food Chem.* **2019**, *270*, 189−195.
(4) Nasabi, M.; Labbafi, M.; Mousavi, M. E.; Madadlou, A. Effect of salts and nonionic surfactants on thermal characteristics of egg white proteins. *Int. J. Biol. Macromol.* **2017**, *102*, 970−976.
(5) Mine, Y. Recent advances in the understanding of egg white protein functionality. *Trends Food Sci. Technol.* **1995**, *6* (7), 225−232.
(6) Kaipparettu, B. A.; Kuiatse, I.; Chan, B. T. Y.; et al. Novel egg white-based 3-D cell culture system. *Biotechniques* **2008**, *45*, 165−171.
(7) Dávalos, A.; Miguel, M.; Bartolomé, B.; López-Fandiño, R. Antioxidant activity of peptides derived from egg white proteins by enzymatic hydrolysis. *J. Food Prot.* **2004**, *67* (9), 1939−1944.
(8) Holen, E.; Bolann, B.; Elsayed, S. Novel B and T cell epitopes of chicken ovomucoid (Gal d 1) induce T cell secretion of IL-6, IL-13, and IFN-gamma. *Clin. Exp. Allergy* **2001**, *31* (6), 952−964.
(9) Mine, Y.; Ma, F.; Lauriau, S. Antimicrobial peptides released by enzymatic hydrolysis of hen egg white lysozyme. *J. Agric. Food Chem.* **2004**, *52* (5), 1088−1094.
(10) Li, Y. J.; Zhang, H. Y.; Zhang, S. R.; et al. Egg White peptide KPHAEVVLR promotes skin fibroblasts migration and mice skin wound healing by stimulating cell membrane Hsp90α secretion. *Process Biochem.* **2020**, *92* (92), 29−36.
(11) Ibrahim, H. R.; Kiyono, T. Novel Anticancer Activity of the Autocleaved Ovotransferrin against Human Colon and Breast Cancer Cells. *J. Agric. Food Chem.* **2009**, *57* (23), 11383−11390.
(12) Kehinde, B. A.; Sharma, P. Recently isolated antidiabetic hydrolysates and peptides from multiple food sources: a review. *Crit. Rev. Food Sci. Nutr.* **2020**, *60* (2), 322−340.
(13) Huang, J.; You, X.; Xin, P.; et al. Egg white as a natural and safe biomaterial for enhanced cancer therapy. *Chin. Chem. Lett.* **2021**, *32* (5), 1737−1742.
(14) Tomczyńska-Mleko, M.; Terpiłowski, K.; Mleko, S. New product development: Cellulose/egg white protein blend fibers. *Carbohydr. Polym.* **2015**, *126*, 168−174.
(15) Zhang, Y. L.; Pham, H. M.; Munguia-Lopez, J. G.; et al. The optimization of a novel hydrogel egg white-alginate for 2.5D tissue engineering of salivary spheroid-like structure. *Molecules* **2020**, *25*, 5751.
(16) Lu, T.; Zou, Q.; Zhu, K. Z.; et al. Electrospun egg white/polyvinyl alcohol fiber dressing to accelerate wound healing. *J. Polym. Res.* **2021**, *28* (2), 1−15.
(17) Zhang, J.; Huang, J.; Huang, K.; et al. Egg white coated alginate nanoparticles with electron sprayer for potential anticancer application. *Int. J. Pharm.* **2019**, *564*, 188−196.
(18) Guo, Z.; Zhang, T.; Fang, K.; et al. The effects of macroporosity and stiffness of poly[(methyl vinyl ether)-alt-(maleic acid)] cross-linked egg white simulations of an aged extracellular matrix on the proliferation of ovarian cancer cells. *RSC Adv.* **2016**, *6*, 43892−43900.
(19) Jalili, F. S.; Rajabi, Z. S.; Mohammadi, P.; et al. Facile fabrication of egg white microporous sponges for tissue regeneration. *Adv. Healthcare Mater.* **2015**, *4* (15), 2281−2290.
(20) Balaji, P.; Perumalsamy, B.; Murugadas, A.; Anbazhagan, M.; Shanmugaapriya, S.; Sellathamby, S. Fabrication and characterization of egg white cryogel scaffold for three-dimensional (3D) cell culture. *Biocatal. Agric. Biotechnol.* **2019**, *17*, 441−446.
(21) Duan, B. C.; Yang, M. H.; Chao, Q. C.; et al. Preparation and properties of egg white dual cross-linked Hydrogel with potential application for bone tissue engineering. *Polymers* **2022**, *14*, 14.
(22) Liu, L. L.; Yang, X. P.; Bhandari, B.; et al. Optimization of the formulation and properties of 3D-printed complex egg white protein objects. *Foods* **2020**, *9* (2), 164.
(23) Huang, K.; Hou, J.; Gu, Z.; Wu, J. Egg-white-/eggshell-based biomimetic hybrid hydrogels for bone regeneration. *ACS Biomater. Sci. Eng.* **2019**, *5* (10), 5384−5391.
(24) Tanaka, K.; Inoue, S.; Mizuno, S. Hydrophobic interaction of P25, containing Asn-linked oligosaccharide chains, with the H-L complex of silk fibroin produced by *Bombyx mori*. *Insect Biochem. Mol. Biol.* **1999**, *29* (3), 269−276.
(25) Murphy, A. R.; David, L. K. Biomedical applications of chemically-modified silk fibroin. *J. Mater. Chem.* **2009**, *19*, 6443−6450.
(26) Kim, S. H.; Yeon, Y. K.; Lee, J. M.; et al. Precisely printable and biocompatible silk fibroin bioink for digital light processing 3D printing. *Nat. Commun.* **2018**, *9*, No. 1620.
(27) Li, J. X.; Zhao, S. X.; Zhang, Y. Q. Silk protein composite bioinks and their 3D scaffolds and in vitro characterization. *Int. J. Mol. Sci.* **2022**, *23* (2), 910.
(28) Zhao, Z. L.; Li, W. W.; Wang, F.; Zhang, Y. Q. Using of hydrated lime water as a novel degumming agent of silk and sericin recycling from wastewater. *J. Cleaner Prod.* **2018**, *172*, 2090−2096.
(29) Wang, H. Y.; Zhang, Y. Q.; Wei, Z. G. Characterization of undegraded and degraded silk fibroin and its significant impact on the properties of the resulting silk biomaterials. *Int. J. Biol. Macromol.* **2021**, *176*, 578−588.
(30) Zhang, M.; Weng, Y. J.; Zhang, Y. Q. Accelerated desalting and purification of silk fibroin in a $CaCl_2$-EtOH-H_2O ternary system by excess isopropanol extraction. *J. Chem. Technol. Biotechnol.* **2021**, *96* (5), 1176−1186.
(31) Sinna, J.; Numpaisal, P. O.; Ruksakulpiwat, C.; Ruksakulpiwat, Y. Extraction of silk fibroin and glycidyl methacrylate grafting on silk fibroin optimization of SF-g-GMA for meniscus tissue engineering. *Mater. Today: Proc.* **2021**, *47*, 3476−3479.
(32) Liu, S.; Zhang, H.; Hu, Q.; et al. Designing vascular supportive albumen-rich composite bioink for organ 3D printing. *J. Mech. Behav. Biomed. Sci.* **2020**, *104*, No. 103642.

https://doi.org/10.1021/acsomega.3c05810
ACS Omega 2023, 8, 46685−46696